Applied Physics Letters ARTICLE scitation.org/journal/apl

Electron overflow of AlGaN deep ultraviolet light emitting diodes

Cite as: Appl. Phys. Lett. **118**, 241109 (2021); doi: 10.1063/5.0055326
Submitted: 28 April 2021 · Accepted: 2 June 2021 ·
Published Online: 17 June 2021

A. Pandey,[1] J. Gim,[2] R. Hovden,[2] and Z. Mi[1,a)]

AFFILIATIONS

[1]Department of Electrical Engineering and Computer Science, University of Michigan, 1301 Beal Avenue, Ann Arbor, Michigan 48109, USA
[2]Department of Materials Science and Engineering, University of Michigan, Ann Arbor, Michigan 48109, USA

[a)]**Author to whom correspondence should be addressed:** ztmi@umich.edu. **Tel.:** (734) 764–3963

ABSTRACT

We have studied the design, epitaxy, and performance characteristics of deep ultraviolet (UV) AlGaN light emitting diodes (LEDs). By combining the tunnel junction and polarization-engineered AlGaN electron blocking layer, a maximum external quantum efficiency and wall-plug efficiency of 0.35% and 0.21%, respectively, were measured for devices operating at ∼245 nm, which are over one order of magnitude higher than previously reported tunnel junction devices at this wavelength. Severe efficiency droop, however, was measured at very low current densities (∼0.25 A/cm^2), which, together with the transverse magnetic (TM) polarized emission, is identified to be the primary limiting factors for the device performance. Detailed electrical and optical analysis further shows that the observed efficiency droop is largely due to an electrical effect instead of an optical phenomenon. Our studies suggest that AlGaN deep UV LEDs with efficiency comparable to InGaN blue-emitting quantum wells can be potentially achieved if issues related to electron overflow and TM polarized emission are effectively addressed.

Ultraviolet (UV)-C semiconductor light emitting diodes (LEDs) are gaining much attention due to their ability to inactivate pathogens, which is essential for water purification, food preservation, and surface sterilization.[1,2] Their ease of use, small size, and low power requirements, compared to conventional mercury and xenon lamps, will enable much broader and widespread application in combating or even possibly preventing another global pandemic. While conventional UV-C devices have been focused on the 260–270 nm wavelength range,[2] recent studies suggested that even shorter wavelengths, i.e., ∼200–220 nm in the far UV-C, are not only more effective at sterilization but can significantly limit the dangers of human exposure to UV radiation due to the shorter penetration depth of higher energy photons in skin.[3] To date, however, such devices exhibit extremely low efficiency due to the low internal quantum efficiency (IQE), insufficient light extraction, and the difficulty in p-doping of ultrawide bandgap AlGaN materials.[4–6] In this regard, tunnel junction-based devices have garnered significant attention, offering a route that can alleviate some of the critical issues associated with the low hole injection by providing a conductive, transparent n-doped layer for enhanced charge carrier (hole) injection, current spreading, and light extraction.[7–13] Large electric fields within the tunnel junction layer can be created through polarization engineering, enabling relatively narrow depletion widths despite the wide bandgap AlGaN materials.[8–18] To realize UV-C LEDs emitting below 250 nm, however, the Al composition of AlGaN needs to be tuned >75%, which causes serious issues for p-type as well as n-type doping.[19–21] These factors not only drastically reduce the probability of the inter-band tunneling of charge carriers across the tunnel junction, but also lead to extremely poor charge carrier (particularly hole) injection. Consequently, the best reported EQE values are well below 0.1% for AlGaN tunnel junction LEDs operating below 250 nm.[7,9]

Recently, significant advances have been made in the molecular beam epitaxy (MBE) of AlGaN and their device applications. With the use of MBE, relatively efficient p-type conduction of Al-rich AlGaN has been achieved through *in situ* surface Fermi level control under slightly Ga-rich epitaxy conditions.[22,23] This growth process also leads to the formation of Ga-rich clusters in AlGaN layers,[16,24–29] which provide highly localized sites for efficient radiative recombination, thereby overcoming the efficiency limitation placed by dislocations.[30] To date, however, there are a few studies of tunnel junction AlGaN deep UV LEDs toward far UV-C emission.[31] Moreover, the currently reported tunnel junction AlGaN deep UV LEDs generally display a

pronounced efficiency droop, even for operation at very low current densities, which limits their high-power applications. Efficiency droop is a well-studied phenomenon in InGaN-based optoelectronic devices, with the underlying causes including Auger recombination,[32–36] electron overflow,[37–39] defect-related mechanisms, carrier delocalization,[40,41] and a combination of these factors.[42] To date, however, the underlying cause for the severe efficiency droop of AlGaN deep UV LEDs has remained largely unexplored.

In this Letter, we report on a detailed study of the design, epitaxy, and performance characteristics of AlGaN tunnel junction deep UV LEDs. By incorporating a Mg-doped, polarization engineered electron blocking layer, a maximum external quantum efficiency and wall-plug efficiency of 0.35% and 0.21%, respectively, were measured for devices operating at ∼245 nm, which are over one order of magnitude higher than previously reported tunnel junction devices at this wavelength.[7,9] Severe efficiency droop, however, was measured at very low current densities (∼0.25 A/cm^2), which, together with the transverse magnetic (TM) polarized emission, are identified to be the primary limiting factors for the performance of AlGaN deep UV LEDs. Detailed electrical and optical analysis further suggests that the observed efficiency droop is largely due to an electrical effect, instead of an optical phenomenon. This study provides insights into how to further improve the efficiency of UV-C and far UV-C LEDs that are relevant for a broad range of applications including water and air purification and sterilization.

AlGaN LED heterostructures were grown on AlN-on-sapphire substrates using a Veeco Gen 930 plasma-assisted MBE system. The epitaxy was performed under slightly Ga-rich conditions at a substrate temperature of ∼750 °C. Three different tunnel junction LED designs, samples A–C, schematically shown in Fig. 1(a), were studied. All the structures consist of an initial bottom n-AlGaN contact layer with a thickness of 500 nm. Immediately preceding the active region, the Al composition of the n-AlGaN layer was graded up from ∼85% to ∼95%. The active region consisted of a single 6 nm thick AlGaN quantum well emitting at ∼245 nm. The use of a single quantum well minimizes the issue of non-uniform carrier injection in the quantum well active region. To pinpoint the effect of electron overflow, the design of the p-doped region was varied between samples A–C. Sample A included a 25 nm Mg-doped AlGaN electron blocking layer immediately following the active region, which was graded from an Al composition of ∼95% to ∼75%. Sample B is identical to sample A, except that the AlGaN electron blocking layer is undoped, relying solely on polarization-induced doping for generation of charge carriers (holes).[10] Previous studies have shown that the scheme of compositional grading can enhance the effective p-type doping of AlGaN layers.[43,44] Sample C is identical to sample A, except that the compositionally graded AlGaN:Mg electron blocking layer is replaced with a uniform $Al_{0.75}Ga_{0.25}N$:Mg layer of the same thickness. Following the AlGaN electron blocking layer, a 25 nm thick p-$Al_{0.75}Ga_{0.25}N$ layer was grown for all three samples. Subsequently, a 5 nm thick GaN layer was grown over the p-doped layer, followed by an n-doped $Al_{0.75}Ga_{0.25}N$ layer, collectively forming the tunnel junction. The thickness of the n-$Al_{0.75}Ga_{0.25}N$ layer is 150 nm to allow adequate current spreading.

Structural properties of sample A were studied by using a JEOL 3100R05 microscope with Cs aberration corrected STEM (300 keV, 22 mrad) and a ADF detector with a camera length of 120 mm and a detector angle of 59 (inner)–354 mrad (outer). The high-angle annular

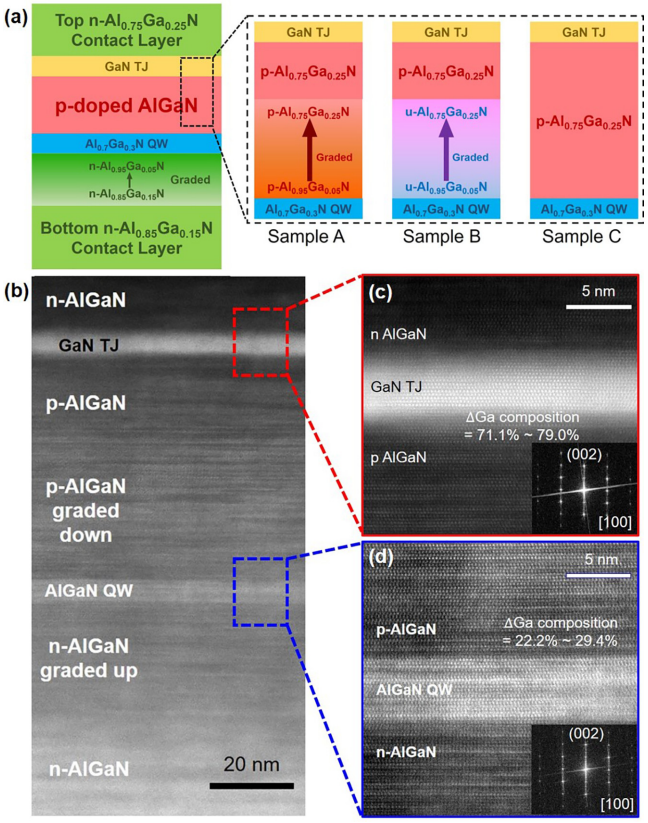

FIG. 1. (a) Schematic of the different tunnel junction UV LED device structures. (b) HAADF-STEM image of the complete device structure of sample A. (c) Atomic-scale HAADF-STEM of the tunnel junction region showing crystalline epitaxial growth of p-AlGaN/GaN/n-AlGaN. (d) Atomic-resolution HAADF-STEM of the AlGaN quantum well active region. FFT shows the superlattice peak associated with Ga-rich atomic ordering (brighter layers in the corresponding HAADF-STEM image) in wurtzite AlGaN along c-plane direction.

dark-field scanning transmission electron microscopy (HAADF-STEM) confirms the cross-sectional device heterostructure for sample A [Fig. 1(b)]. Atomic-resolution cross-sectional STEM in Fig. 1(c) reveals the GaN layer (∼5 nm) epitaxially grown between the top n^+-AlGaN and p-AlGaN layer. Relative gallium concentration is determined by the HAADF intensity along [100] approximated by $I_{HAADF} = t \cdot [(f_{Ga}Z_{Ga} + f_{Al}Z_{Al})^{\gamma} + Z_N{}^{\gamma}]$, where I_{HAADF} is the high-angle annular dark field intensity, t is the cross section thickness, f is the concentration of Ga or Al in the AlGaN multilayers, Z is the atomic number of Al, Ga, or N in the layers, and γ is between 1.4 and 1.7. The ratio of HAADF STEM intensity estimates ∼75.0% ± 4.0% less Ga in the p-AlGaN layers compared with the Ga concentration in the GaN layer. Figure 1(d) also shows the epitaxial growth of AlGaN quantum well (∼6 nm) with ∼25.8% ± 3.6% higher content of Ga relative to adjacent AlGaN barriers in the graded active region. The brighter atomic layers in the active region corresponding to the Ga-rich layers reveal significant compositional non-uniformity in the epilayers due to the use of slight metal-rich epitaxy conditions. Fast Fourier transform (FFT) patterns of the HAADF-STEM images also

exhibit ordering of a Ga-rich layer along the [001] direction, which are forbidden in the electron diffraction pattern of wurtzite hexagonal symmetry. The formation of extensive nanoscale AlGaN clusters can provide three-dimensional quantum-confinement of charge carriers, which was shown to dominate the EL of MBE-grown AlGaN UV LEDs[16] and is the principle mechanism for the enhanced internal quantum efficiency for AlGaN grown by PA-MBE.[24,27,45–47]

For the UV LED fabrication, first ion milling was used to etch down to the bottom n-AlGaN layer to make the device mesas. 300 nm of SiO_2 was deposited using PECVD for insulation. Reactive ion etching, with high selectivity between AlGaN and SiO_2, was used to etch vias in the insulation layer for the deposition of metal contacts. A Ti/Al/Ni/Au metal stack was deposited onto the exposed top and bottom n-AlGaN for the device contacts. Annealing of the contacts was performed in a nitrogen ambient at 700 °C for 30 s. Al/Au metal contact pads were deposited over the annealed device contacts to facilitate electrical probing and measurements.

The electrical properties of the devices were measured under continuous-wave (CW) biasing conditions using a Keithley 2400 SMU. The J–V characteristics of representative devices are shown in Fig. 2(a). Sample B, which relies solely on polarization doping, is observed to be leaky, while samples A and C show excellent rectifying characteristics. This indicates that a proper p-n junction was not formed in sample B. Sample A exhibits a higher turn-on voltage compared to sample C; however, the turn-on is significantly sharper for sample A. Severe electron overflow can result in an earlier, but more gradual, turn-on voltage for LEDs, indicating that electron overflow is better controlled in sample A, due to the polarization engineered electron blocking layer.[10] Samples A and C show very similar characteristics at high forward bias, indicating that they have similar device resistances. The ideality factor calculated for samples A–C is 7.74, 18.15, and 12.48, respectively. The relatively high ideality factors are a consequence of the presence of a tunnel junction in the devices, as well as the hole transport being dominated by tunneling within an impurity band of AlGaN.[23,48,49] However, since all three devices have identical tunnel junction design, the significant differences in the measured ideality factors may be a result of other factors. Higher ideality factors have been associated with insufficient doping, higher layer resistances, and increased electron overflow.[50,51] From these measurements, we conclude that the polarization-engineered AlGaN:Mg electron blocking layer plays a crucial role in charge carrier transport, and its presence is beneficial to improved current-voltage characteristics.

We further measured the EL spectra, shown in Fig. 2(b), under similar current injections around 40 A/cm^2 for all three samples. The peak of the EL spectrum is measured at ∼245 nm for all the samples. Samples A and C exhibit relatively bright luminescence, however, the luminescence from sample B is significantly weaker. The full-width half maximum (FWHM) is measured to be ∼15 nm for sample A, which is comparable to previously reported LEDs grown by MBE.[8,11,12,16] Sample B has a similar FWHM although it also exhibits a shoulder at shorter wavelengths close to 235 nm, suggesting that there is significant recombination of charge carriers within the higher Al content layers of the device. Sample C has a significantly broader emission peak with FWHM over 25 nm. The wide emission peak is a strong indication of more severe electron overflow in this device. Further, sample C also shows a relatively long tail as compared to the other devices, which can be explained by emission from the Mg

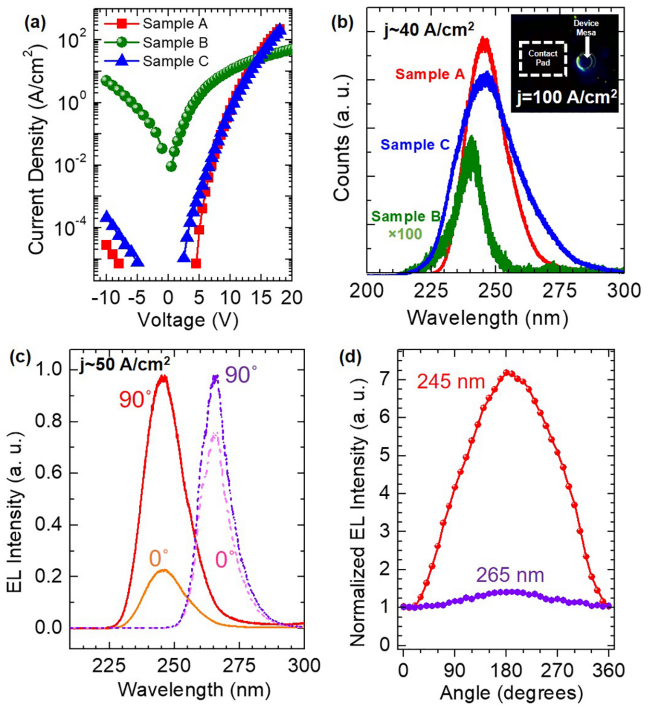

FIG. 2. (a) J–V characteristics of the different tunnel junction UV LED device structures. (b) Room-temperature electroluminescence spectra measured for the different devices under current injection densities ∼40 A/cm^2. The electroluminescence of sample B has been magnified by a factor of 100. The inset shows a device from sample A under an injection current of ∼100 A/cm^2. (c) Electroluminescence spectra measured at polarization angles of 0° and 90° for sample A (245 nm), shown as solid curves, and an identical device with emission at 265 nm, shown as dashed curves. (d) Variation of electroluminescence intensity with polarization angle measured for sample A (245 nm) in red, and an identical device with emission at 265 nm in purple.

acceptor related transition of the p-doped $Al_{0.75}Ga_{0.25}N$[23]. The inset of Fig. 2(b) shows a device from sample A under an injection current of 100 A/cm^2. It is seen that there is a significant amount of light being emitted from the edges of the device mesa, despite the metal contact completely covering the top of the device.

We studied the emission polarization properties of sample A as well as an LED with an identical structure but having emission at 265 nm. The samples were placed under a constant CW bias corresponding to an injected current density of ∼50 A/cm^2. A Glan–Taylor calcite polarizer with a high-precision rotation mount system was placed on the sample top surface to resolve the emission. Figure 2(c) plots the EL spectra for the two devices at polarization angles of 0° and 90°. A much larger change in intensity was seen for the 245 nm LED as compared to the 265 nm device, suggesting a significantly larger degree of polarization. This is consistent with previous studies that reported the light emission becoming more TM polarized for higher Al compositions.[52] The variation of the EL intensity, normalized to the minimum value for each device, with polarization angle for the two devices is shown in Fig. 2(d). The degree of polarization was measured to be −0.602 and −0.078 for the 245 and 265 nm LEDs, respectively, which confirms a major shift toward emission that is

dominantly TM-polarized with decreasing wavelengths. It is therefore expected that the device efficiency can be significantly enhanced by engineering the polarization of the light emission to be more TE-like,[53–55] by utilizing nanostructures,[56–60] and/or by removing the substrate.[61–63]

The output power was measured from the bottom of the sapphire substrate using a Newport 818-ST2-UV photodetector with a Newport Model 1919-R power meter. The devices were probed under CW biasing conditions. Figures 3(a) and 3(b) show the variation of EQE and WPE, respectively, with current density for samples A and C. The maximum EQE and WPE for sample A are 0.35% and 0.21%, respectively, at a current density of 0.25 A/cm^2. The peak EQE and WPE of sample A is over 50% higher than that of sample C. In fact, the measured efficiency values are more than one order of magnitude higher than previously reported tunnel junction devices at these wavelengths.[7,9,12] Sample B exhibited extremely low efficiency (∼0.001%) due to the leaky I–V, which is not shown here. Given that both samples A and C have identical active region and tunnel junction designs, the improved performance of sample A can be well explained by the incorporation of a polarization engineered p-AlGaN EBL layer, which can help reduce electron overflow and enhance the device efficiency. This observation is also consistent with the enhanced electron overflow of sample C derived from electrical analysis, as described above. The underlying cause for the severe electron overflow is due the highly asymmetric electron and hole transport properties of Al-rich AlGaN,[8,9,16] which fundamentally limits the maximum achievable efficiency of deep UV LEDs.

It is also noticed that similar efficiency droop phenomena have been measured in AlGaN LEDs operating at 255–280 nm wavelengths.[8,9,16] To further confirm if the observed efficiency droop is due to an electrical effect, we studied the optical properties of the AlGaN quantum well active region (∼265 nm), schematically shown in Fig. 4(a), to determine if it plays a significant role in the efficiency droop process. Figure 4(b) shows the PL spectrum measured by exciting the sample using a 193 nm Coherent Excistar XS500 laser. It shows the presence of two peaks: one located at ∼240 nm, originating from the high Al-content barrier layers, and another at ∼268 nm, originating from the quantum wells. To study only the luminescence from the quantum wells and avoid the effects of carrier transport between the wells and barriers, the sample was resonantly excited using a frequency-tripled Ti:sapphire laser (∼245 nm) with an 80 MHz repetition rate and 100 fs pulse width. The excitation power was varied over several orders of magnitude, and the PL spectra are shown in Fig. 4(c). The relative EQE is shown in Fig. 4(d), exhibiting no significant droop

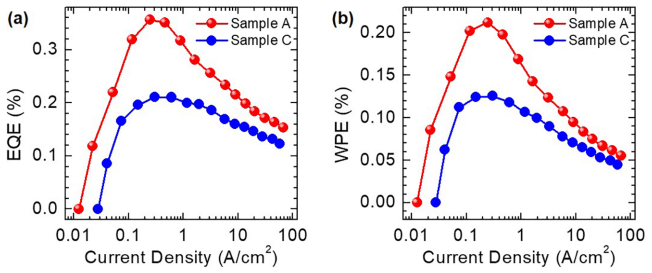

FIG. 3. (a) EQE vs current density of sample A and C, measured using CW bias. (b) WPE vs current density of sample A and C, measured using CW bias.

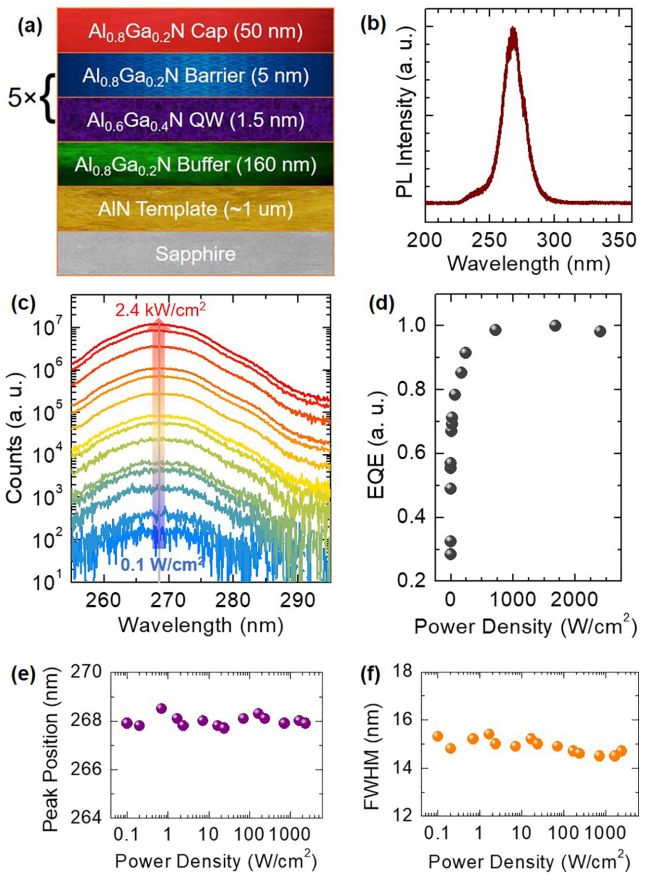

FIG. 4. (a) Structure of the sample used for optical measurements. (b) Room-temperature photoluminescence spectra for the structure measured using 193 nm excitation. (c) Intensity-dependent photoluminescence spectra measured for the sample using quasi-resonant excitation of the active region. (d) Relative EQE measured for optical emission at different excitation powers. (e) Variation of peak position with excitation power density. (f) Plot of measured full-width half maximum for the emission peak at different excitation power densities.

up to an excitation power of 2.4 kW/cm^2, which corresponds to an estimated carrier density of $\sim 2 \times 10^{18}$ cm^{-3}.[35,64,65] A negligible change in peak position was seen over this wide excitation range, shown in Fig. 4(e), suggesting that the emission is a result of the radiative recombination of highly confined and localized carriers. The linewidth of the emission, plotted against excitation power in Fig. 4(f), remains almost constant throughout the excitation range, showing negligible quantum-confined Stark effect.

TRPL transients were also collected at different optical excitation powers using a thermoelectrically cooled fast hybrid photomultiplier tube. Some representative transients are shown in Fig. 5(a), which exhibit an almost negligible change in their decay over the excitation range. Figure 5(b) plots the extracted carrier lifetimes by using the stretched-exponential model.[29,66] The nearly invariant carrier lifetime (∼0.3 ns) shows that the carrier recombination dynamics do not change significantly over the excitation range, suggesting that higher order carrier loss processes, e.g., Auger recombination, is not significant in the measured excitation power range. Auger recombination would

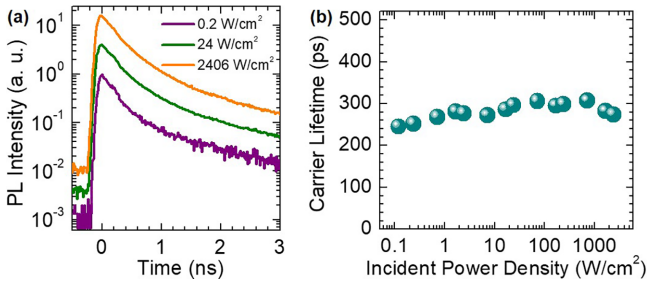

FIG. 5. (a) Time-resolved photoluminescence decays at different excitation powers collected for the sample used in optical measurements. (b) Plot of extracted carrier lifetime vs excitation power density.

cause an increase in non-radiative emission and a decrease in carrier lifetime when the excitation power is increased.[35,64,65] The carrier lifetimes measured were comparable to previously reported high quality AlGaN epilayers grown by MBE.[67] It is also noteworthy that the extracted carrier lifetimes are significantly lower than those measured for AlGaN quantum wells grown by metal-organic chemical vapor deposition (MOCVD),[35] which can be explained by the strong quantum-confinement of charge carriers in the quantum dot-like nanoclusters for samples grown by plasma-assisted MBE. In addition, recent studies have shown that the exciton binding energy can be significantly enhanced in AlGaN nanostructures, which also contribute to the reduced radiative lifetime.[68,69] Furthermore, no evidence of droop is observed in the optical measurements up to an estimated carrier density of $\sim 2 \times 10^{18}\,\mathrm{cm}^{-3}$. For comparison, previously reported blue-emitting InGaN quantum wells[65] also did not display any efficiency droop up to carrier densities $\sim 5 \times 10^{18}\,\mathrm{cm}^{-3}$, which approximately corresponds to injection current densities 5–15 A/cm^2. Given the shorter carrier lifetime measured in the presented AlGaN active region, the carrier density of $\sim 2 \times 10^{18}\,\mathrm{cm}^{-3}$ would correspond to a higher current density than that observed in InGaN LEDs for the onset of efficiency droop.[29,65,68,70] Therefore, it is reasonable to conclude the measured efficiency droop in electroluminescence at $\sim$0.25 A/cm^2 is not an optical phenomenon, but instead related to an electrical origin, i.e., electron overflow.

In conclusion, we have demonstrated AlGaN deep UV tunnel junction LEDs operating at $\sim$245 nm, which exhibit significantly improved efficiency compared to previous reports. Severe efficiency droop was measured at low current densities. Detailed electrical and optical studies suggest that the efficiency droop is directly related to electron overflow, instead of an optical phenomenon. Moreover, the MBE grown AlGaN deep UV LED active region is characterized with the presence of nanoscale clusters. The resulting strong three-dimensional confinement of charge carriers can significantly reduce the quantum-confined Stark effect, leading to highly stable and efficient emission. Our studies further suggest that AlGaN deep UV LEDs with efficiency comparable to InGaN blue-emitting quantum wells can be potentially achieved if issues related to electron overflow and TM polarized emission are effectively addressed.

This work was supported by the Blue Sky research program in the College of Engineering at the University of Michigan and National Science Foundation (Grant No. DMR-1807984). Some intellectual property related to this work was licensed to NS Nanotech Inc., which was co-founded by Z. Mi.

DATA AVAILABILITY

The data that support the findings of this study are available from the corresponding author upon reasonable request.

REFERENCES

[1]V. M. Gomez-Lopez, P. Ragaert, J. Debevere, and F. Devlieghere, Trends Food Sci. Technol. **18**(9), 464–473 (2007).
[2]T. Dai, M. S. Vrahas, C. K. Murray, and M. R Hamblin, Expert Rev. Anti-Infect. Ther. **10**(2), 185–195 (2012).
[3]M. Buonanno, D. Welch, I. Shuryak, and D. J. Brenner, Scientific Reports **10**(1), 10285 (2020).
[4]Y. Nagasawa and A. Hirano, Appl. Sci. **8**(8), 1264 (2018).
[5]A. Khan, K. Balakrishnan, and T. Katona, Nat. Photonics **2**(2), 77–84 (2008).
[6]H. Hirayama, S. Fujikawa, and N. Kamata, Electron. Commun. Jpn. **98**(5), 1–8 (2015).
[7]S. Bharadwaj, K. Lee, S. Islam, V Protasenko, H. G Xing, and D. Jena, in presented at the CLEO: Science and Innovations (2017) (unpublished).
[8]A. Pandey, W. J. Shin, J. Gim, R. Hovden, and Z. Mi, Photonics Res. **8**(3), 331–337 (2020).
[9]S. Sadaf, S. Zhao, Y. Wu, Y.-H. Ra, X. Liu, S. Vanka, and Z. Mi, Nano Lett. **17**(2), 1212–1218 (2017).
[10]Y. Zhang, S. Krishnamoorthy, F. Akyol, A. A. Allerman, M. W. Moseley, A. M. Armstrong, and S. Rajan, Appl. Phys. Lett. **109**(19), 191105 (2016).
[11]Y. Zhang, Z. Jamal-Eddine, F. Akyol, S. Bajaj, J. M. Johnson, G. Calderon, A. A. Allerman, M. W. Moseley, A. M. Armstrong, and J. Hwang, Appl. Phys. Lett. **112**(7), 071107 (2018).
[12]Y. Zhang, S. Krishnamoorthy, F. Akyol, S. Bajaj, A. A. Allerman, M. W. Moseley, A. M. Armstrong, and S. Rajan, Appl. Phys. Lett. **110**(20), 201102 (2017).
[13]C. Kuhn, L. Sulmoni, M. Guttmann, J. Glaab, N. Susilo, T. Wernicke, M. Weyers, and M. Kneissl, Photonics Res. **7**(5), B7–B11 (2019).
[14]M. F. Schubert, Physical Review B **81**(3), 035303 (2010).
[15]S. Krishnamoorthy, D. N. Nath, F. Akyol, P. S. Park, M. Esposto, and S. Rajan, Appl. Phys. Lett. **97**(20), 203502 (2010).
[16]A. Pandey, J. Gim, R. Hovden, and Z. Mi, Appl. Phys. Lett. **117**(24), 241101 (2020).
[17]J. Simon, Z. Zhang, K. Goodman, H. Xing, T. Kosel, P. Fay, and D Jena, Phys. Rev. Lett. **103**(2), 026801 (2009).
[18]Y. Zhang, S. Krishnamoorthy, J. M. Johnson, F. Akyol, A. Allerman, M. W. Moseley, A. Armstrong, J. Hwang, and S. Rajan, Appl. Phys. Lett. **106**(14), 141103 (2015).
[19]R. Collazo, S. Mita, J. Xie, A. Rice, J. Tweedie, R. Dalmau, and Z. Sitar, Phys. Status Solidi C **8**(7–8), 2031–2033 (2011).
[20]B. Sarkar, S. Washiyama, M. H. Breckenridge, A. Klump, J. N. Baker, P. Reddy, J. Tweedie, S. Mita, R. Kirste, and D. L. Irving, ECS Trans. **86**(12), 25 (2018).
[21]Y. Taniyasu, M. Kasu, and N. Kobayashi, Appl. Phys. Lett. **81**(7), 1255–1257 (2002).
[22]X. Liu, A. Pandey, D. A. Laleyan, K. Mashooq, E. T. Reid, W. J. Shin, and Z. Mi, Semicond. Sci. Technol. **33**(8), 085005 (2018).
[23]A. Pandey, X. Liu, Z. Deng, W. Shin, D. Laleyan, K. Mashooq, E. Reid, E. Kioupakis, P. Bhattacharya, and Z. Mi, Phys. Rev. Mater. **3**(5), 053401 (2019).
[24]A. Bhattacharyya, T. Moustakas, L. Zhou, D. J. Smith, and W. Hug, Appl. Phys. Lett. **94**(18), 181907 (2009).
[25]M. Gao, S. Bradley, Y. Cao, D. Jena, Y. Lin, S. Ringel, J. Hwang, W. Schaff, and L. Brillson, Journal of Applied Physics **100**(10), 103512 (2006).
[26]V. N. Jmerik, E. V. Lutsenko, and S. V. Ivanov, Physica Status Solidi (a) **210**(3), 439–450 (2013).
[27]T. D. Moustakas and A. Bhattacharyya, Phys. Status Solidi C **9**(3–4), 580–583 (2012).
[28]T. D. Moustakas, Y. Liao, C.-K. Kao, C. Thomidis, A. Bhattacharyya, D. Bhattarai, and A. Moldawer, in presented at the Light-Emitting Diodes: Materials, Devices, and Applications for Solid State Lighting XVI (2012) (unpublished).
[29]A. Aiello, A. Pandey, A. Bhattacharya, J. Gim, X. Liu, D. A. Laleyan, R. Hovden, Z. Mi, and P. Bhattacharya, J. Cryst. Growth **508**, 66–71 (2019).

[30]J. Speck and S Rosner, Physica B **273–274**, 24–32 (1999).
[31]S. Zhao, S. Sadaf, S. Vanka, Y. Wang, R. Rashid, and Z Mi, Appl. Phys. Lett. **109**(20), 201106 (2016).
[32]J. Piprek, Phys. Status solidi A **207**(10), 2217–2225 (2010).
[33]J. Cho, E. F. Schubert, and J. K. Kim, Laser Photonics Rev. **7**(3), 408–421 (2013).
[34]J. Iveland, L. Martinelli, J. Peretti, J. S. Speck, and C. Weisbuch, Phys. Rev. Lett. **110**(17), 177406 (2013).
[35]F. Nippert, M. Tollabi Mazraehno, M. J. Davies, M. P. Hoffmann, H.-J. Lugauer, T. Kure, M. Kneissl, A. Hoffmann, and M. R. Wagner, Appl. Phys. Lett. **113**(7), 071107 (2018).
[36]C. Frankerl, F. Nippert, A. Gomez-Iglesias, M. P. Hoffmann, C. Brandl, H.-J. Lugauer, R. Zeisel, A. Hoffmann, and M. J. Davies, Appl. Phys. Lett. **117**(10), 102107 (2020).
[37]X. Hai, R. Rashid, S. Sadaf, Z. Mi, and S. Zhao, Appl. Phys. Lett. **114**(10), 101104 (2019).
[38]J. Yun, J.-I. Shim, and H. Hirayama, Appl. Phys. Express **8**(2), 022104 (2015).
[39]C. Chu, K. Tian, J. Che, H. Shao, J. Kou, Y. Zhang, Z.-H. Zhang, and H.-C. Kuo, IEEE Photonics J. **12**(3), 1–7 (2020).
[40]J. Mickevičius, G. Tamulaitis, M. Shur, M. Shatalov, J. Yang, and R Gaska, Appl. Phys. Lett. **101**(21), 211902 (2012).
[41]J. Mickevičius, G. Tamulaitis, M. Shur, M. Shatalov, J. Yang, and R. Gaska, Appl. Phys. Lett. **103**(1), 011906 (2013).
[42]H.-H. Chen, J. S. Speck, C. Weisbuch, and Y.-R. Wu, Appl. Phys. Lett. **113**(15), 153504 (2018).
[43]D. Jena, J. Simon, A. Wang, Y. Cao, K. Goodman, J. Verma, S. Ganguly, G. Li, K. Karda, and V. Protasenko, Phys. Status Solidi A **208**(7), 1511–1516 (2011).
[44]J. Simon, V. Protasenko, C. Lian, H. Xing, and D. Jena, Science **327**(5961), 60–64 (2010).
[45]Y. Liao, C. Thomidis, C.-K. Kao, and T. D. Moustakas, Appl. Phys. Lett. **98**(8), 081110 (2011).
[46]T. D. Moustakas, MRS Commun. **6**(3), 247–269 (2016).
[47]Y.-H. Liang, N. T. Nuhfer, and E. Towe, J. Vac. Sci. Technol. B **34**(2), 02L112 (2016).
[48]N. Bochkareva, V. Voronenkov, R. Gorbunov, A. Zubrilov, Y. S. Lelikov, P. Latyshev, Y. Rebane, A. Tsyuk, and Y. Shreter, Appl. Phys. Lett. **96**(13), 133502 (2010).
[49]T. Kinoshita, T. Obata, H. Yanagi, and S.-I. Inoue, Appl. Phys. Lett. **102**(1), 012105 (2013).
[50]K. Lee, P. Parbrook, T. Wang, J. Bai, F. Ranalli, R. Airey, and G Hill, Phys. Status Solidi B **247**(7), 1761–1763 (2010).
[51]J. M. Shah, Y.-L. Li, T. Gessmann, and E. F. Schubert, J. Appl. Phys. **94**(4), 2627–2630 (2003).
[52]T. Kolbe, A. Knauer, C. Chua, Z. Yang, S. Einfeldt, P. Vogt, N. M. Johnson, M. Weyers, and M. Kneissl, Appl. Phys. Lett. **97**(17), 171105 (2010).
[53]T. Kolbe, A. Knauer, C. Chua, Z. Yang, V. Kueller, S. Einfeldt, P. Vogt, N. M. Johnson, M. Weyers, and M. Kneissl, Appl. Phys. Lett. **99**(26), 261105 (2011).
[54]J. Northrup, C. Chua, Z. Yang, T. Wunderer, M. Kneissl, N. Johnson, and T. Kolbe, Appl. Phys. Lett. **100**(2), 021101 (2012).
[55]C. Reich, M. Guttmann, M. Feneberg, T. Wernicke, F. Mehnke, C. Kuhn, J. Rass, M. Lapeyrade, S. Einfeldt, and A. Knauer, Appl. Phys. Lett. **107**(14), 142101 (2015).
[56]B. Le, X. Liu, N. Tran, S. Zhao, and Z. Mi, Opt. Express **27**(4), 5843–5850 (2019).
[57]K. Li, X. Liu, Q. Wang, S. Zhao, and Z Mi, Nat. Nanotechnol. **10**(2), 140 (2015).
[58]X. Liu, B. H. Le, S. Y. Woo, S. Zhao, A. Pofelski, G. A. Botton, and Z. Mi, Opt. Express **25**(24), 30494–30502 (2017).
[59]X. Liu, K. Mashooq, D. A. Laleyan, E. T. Reid, and Z. Mi, Photonics Res. **7**(6), B12–B23 (2019).
[60]X. Liu, K. Mashooq, T. Szkopek, and Z. Mi, IEEE Photonics J. **10**(4), 1–11 (2018).
[61]J. Kim, C. Bayram, H. Park, C.-W. Cheng, C. Dimitrakopoulos, J. A. Ott, K. B. Reuter, S. W. Bedell, and D. K. Sadana, Nat. Commun. **5**(1), 1–7 (2014).
[62]W. Guo, R. Kirste, I. Bryan, Z. Bryan, L. Hussey, P. Reddy, J. Tweedie, R. Collazo, and Z. Sitar, Appl. Phys. Lett. **106**(8), 082110 (2015).
[63]W. Wong, T. Sands, N. Cheung, M. Kneissl, D. Bour, P. Mei, L. Romano, and N. Johnson, Appl. Phys. Lett. **75**(10), 1360–1362 (1999).
[64]W. Guo, M. Zhang, P. Bhattacharya, and J. Heo, Nano Lett. **11**(4), 1434–1438 (2011).
[65]Y. Shen, G. Mueller, S. Watanabe, N. Gardner, A. Munkholm, and M. Krames, Appl. Phys. Lett. **91**(14), 141101 (2007).
[66]R. Chen, J. Lumin. **102–103**, 510–518 (2003).
[67]C. Collins, A. Sampath, G. Garrett, W. Sarney, H. Shen, M. Wraback, A. Y. Nikiforov, G. Cargill III, and V. Dierolf, Appl. Phys. Lett. **86**(3), 031916 (2005).
[68]A. Aiello, Y. Wu, A. Pandey, P. Wang, W. Lee, D. Bayerl, N. Sanders, Z. Deng, J. Gim, and K. Sun, Nano Lett. **19**(11), 7852–7858 (2019).
[69]A. Aiello, Y. Wu, Z. Mi, and P. Bhattacharya, Appl. Phys. Lett. **116**(6), 061104 (2020).
[70]R. Hui and M. O'Sullivan, *Fiber Optic Measurement Techniques* (Academic Press, 2009).